High-pressure Raman study and lattice dynamical calculations for $SrWO_4$

2002 J. Phys.: Condens. Matter 14 12641

(http://iopscience.iop.org/0953-8984/14/47/334)

INSTITUTE OF PHYSICS PUBLISHING JOURNAL OF PHYSICS: CONDENSED MATTER

J. Phys.: Condens. Matter **14** (2002) 12641–12650 PII: S0953-8984(02)34298-X

High-pressure Raman study and lattice dynamical calculations for $SrWO_4$

D Christofilos[1,4], K Papagelis[2,5], S Ves[2], G A Kourouklis[1] and C Raptis[3]

[1] Division of Physics, School of Technology, Aristotle University of Thessaloniki, Thessaloniki 54006, Greece
[2] Physics Department, Aristotle University of Thessaloniki, Thessaloniki 54006, Greece
[3] Department of Physics, National Technical University, Athens 15780, Greece

E-mail: christof@vergina.eng.auth.gr

Received 27 February 2002, in final form 15 October 2002
Published 15 November 2002
Online at stacks.iop.org/JPhysCM/14/12641

Abstract

A high-pressure Raman study of $SrWO_4$ reveals a pressure induced phase transition starting at 11.5 GPa. Several Raman lines exhibit a nonlinear behaviour in the pressure range of 11.5–15 GPa, which can be attributed to either stabilization of the high-pressure phase or an intermediate phase. Using a theoretical lattice dynamical calculation, based on an empirical potential model, we have obtained the Raman active mode eigenvectors giving us an insight into the phase transition mechanism. The lowest-frequency mode exhibits a negative pressure slope in the scheelite phase and involves a motion of the WO_4 tetrahedron as a whole according to the theoretical results. The experimental evidence suggests that the structure of the high-pressure phase is closely related to the scheelite structure, being formed by closely lying distorted WO_4 tetrahedra rather than involving an octahedrally coordinated W ion.

1. Introduction

Tungstate and molybdate divalent scheelites form a well known family of materials which, besides their geological interest [1], are used as host crystals for rare earth ions in solid state laser applications [2] and appear also promising as materials for Raman lasers [3]. The strong interest in their structural stability under hydrostatic pressure is evident by the number of high-pressure Raman [4–8] and x-ray diffraction studies [8–10]. It has been proposed [11] that members of this family undergo a pressure induced phase transition towards the wolframite ($NiWO_4$) structure, which is justified by a tendency of smaller-radius cations to crystallize in this monoclinic structure at ambient conditions. However, x-ray investigations in $CdMoO_4$ and

[4] Author to whom any correspondence should be addressed.
[5] Current address: School of Chemistry, Physics and Environmental Science, University of Sussex, Brighton BN1 9QJ, UK.

$SrMoO_4$ reveal that these compounds respond differently to pressure: the first transforms to the wolframite structure [9] while the second to a different monoclinic structure [8]. Theoretical lattice dynamics calculations based on the rigid-ion model (RIM) have been performed for $CaZnF_4$ [12], $YLiF_4$ and $YbLiF_4$ [13] as well as $CaWO_4$ [14]. These studies have been focused on the phonon dispersion curves as well as bond hierarchy while the mode eigenvectors, which would have been very useful for an unambiguous interpretation of the Raman spectrum and its pressure evolution, have not been calculated in any of the above theoretical studies. These calculations show a very strong Zn–F force constant while the corresponding Li–F interaction in $YLiF_4$ appears weaker. On the other hand, experimental measurements in $CaZnF_4$ [12] and $YLiF_4$ [15] reveal a strong ionic character of the interactions among the atoms and therefore these materials are not analogous to $SrWO_4$. In contrast, the structural parameters of $CaWO_4$ [11] and its behaviour under pressure [6] resemble closely those of $SrWO_4$.

$SrWO_4$ has a tetragonal structure, isomorphic to scheelite ($CaWO_4$) belonging to the $I4_1/a$ (C^6_{4h}) space group with two chemical units in the primitive cell. The fractional atomic coordinates in the primitive cell used for the $SrWO_4$ structure are those of $CaWO_4$, Ca (0, 0.25, 0.625), W (0, 0.25, 0.125), O (0.15, 0.009, 0.211), taking of course the cell parameters $a = b = 5.4168$ Å and $c = 11.951$ Å of $SrWO_4$ [10, 11, 16]. Apart from the three acoustic modes the remaining 33 optical modes belong to the following symmetry species: $\Gamma = 3A_g + 5B_g + 5E_g + 4A_u + 3B_u + 4E_u$. They can be grouped into external and internal modes taking into account that internal modes originate from the WO_4 tetrahedral units [17]. The latter modes span the frequency range 250–921 cm^{-1} with a frequency gap between 380 and 800 cm^{-1} while the external modes (rotational and translational) lie between 75 and 250 cm^{-1} [18]. Previous high-pressure Raman studies of $SrWO_4$ were either restricted to a low-pressure range, and therefore the pressure induced phase transition was not observed at all [4], or, although extended to higher pressures, the relevant investigation involved only three internal modes [6] from which a phase transition at 11.5 GPa was concluded.

In this study, we extend our high-pressure Raman investigation of $SrWO_4$ up to 21 GPa, covering all Raman active modes, well within the high-pressure phase. Our experimental findings are discussed in the light of theoretical calculations of the Raman frequencies and eigenvectors based on a simple empirical Lennard-Jones potential. Furthermore, by considering our experimental data on $SrWO_4$ as well as analogous data on other scheelite-type compounds we propose a possible mechanism of the occurring phase transition and accordingly the possible candidates for the high-pressure induced structures. Details of the experiments have been given elsewhere [6]. The crystals were grown at AT&T and Bell Laboratories and were kindly made available to us by Dr A Jayaraman.

2. Experimental results

Raman spectra of $SrWO_4$ at several pressures and room temperature are shown in figure 1. Only 11 out of the 13 modes are resolved at ambient pressure. The weak line at 171 cm^{-1}, not resolved at ambient pressure and corresponding to the B_g symmetry, gains relative intensity only at higher pressure. The peak at 337 cm^{-1}, attributed to the $A_g(\nu_2)$ and $B_g(\nu_2)$ internal modes, splits into two components only close to the onset of the pressure induced phase transition. Easily noticeable are also the negative pressure coefficient of the lowest-frequency B_g mode of the lower-pressure phase and its reversal at higher pressure as well as the peculiar behaviour of the two internal modes around 820 cm^{-1}.

The pressure dependence of the observed Raman peak frequency is displayed in figure 2. The frequency values are obtained by fitting Lorentzian line shapes to the experimental data. A sample with a naturally cleaved surface, used in one of the runs, permitted us to record

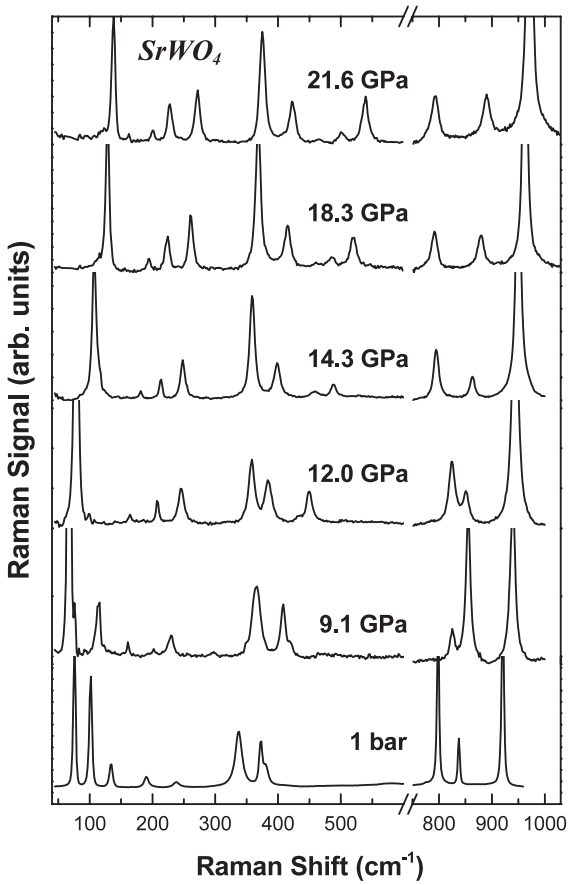

Figure 1. Raman spectra of $SrWO_4$ for various pressures at room temperature.

polarized Raman spectra where only modes with A_g and B_g symmetry were observed. We followed their pressure behaviour for pressures up to ∼18 GPa. These modes are presented in figure 2 by using the same symbols throughout the pressure range investigated, while the continuous curves are drawn to guide the eye through their pressure dependence. The shaded area from 11.5 to 15 GPa marks the pressure range where several of the observed Raman bands exhibit strong nonlinear behaviour in their pressure response. Above 15 GPa, 12 Raman peaks are observed, all of them exhibiting a linear response to pressure.

In the pressure dependence of the modes (figure 2) several features are easily observed.

(i) The two indistinguishable $A_g(\nu_2)$ and $B_g(\nu_2)$ modes at 337 cm^{-1} are well resolved around 10 GPa. This can be considered as a precursor of the structural transition of the scheelite structure occurring at ∼11.5 GPa.
(ii) The negative pressure coefficient of the low-frequency $B_g(T)$ mode in the scheelite phase and its reversal in the high-pressure phase.
(iii) The nonlinear behaviour of several modes in the shaded area of the figure and especially that of $B_g(\nu_3)$, $B_g(\nu_4)$ and the low-frequency $B_g(T)$ mode.
(iv) The $B_g(\nu_3)$ mode exhibits a softening and crossing tendency with the $E_g(\nu_3)$ mode, as is revealed by the polarized spectra. All these effects are fully reversible for pressures up to ∼21 GPa when pressure is released, as can be deduced from figure 2.

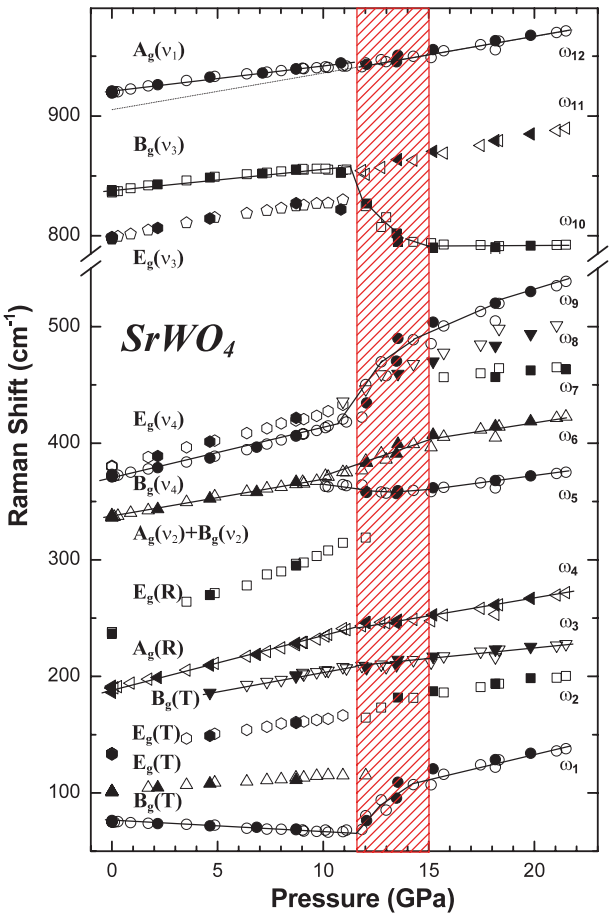

Figure 2. Pressure dependence of the Raman modes of $SrWO_4$ with their assignment for the scheelite structure. Open symbols represent data taken upon increasing pressure whereas solid symbols correspond to downstroke measurements. Solid curves are drawn to guide the eye for the A_g and B_g scheelite modes that were followed in the high-pressure phase in polarized Raman measurements. The dotted curve refers to the extrapolation at ambient pressure of the high-pressure trend of the A_g (ν_1) mode. In the shaded area, from 11.5 to 15 GPa, several modes exhibit a nonlinear behaviour with pressure.

(This figure is in colour only in the electronic version)

The various parameters of the experimental data shown in figure 2, namely frequency, pressure coefficients and Grüneisen parameters for the scheelite structure along with the corresponding values for the high-pressure phase are listed in table 1.

3. Model calculations

In order to obtain a deeper insight into the normal modes in $SrWO_4$ at ambient conditions, we have performed a simple lattice dynamical calculation, with emphasis on the calculation of the eigenvectors and, to a lesser degree, on the calculation of their frequency values. In our model, we assume that any two atoms κ and κ' in the crystal, up to the second neighbours, are

Table 1. Experimental frequencies, pressure coefficients and Grüneisen parameters of the Raman active modes of $SrWO_4$ in the scheelite and the high-pressure phase. Theoretically calculated frequencies ω_{cal}, along with their relative deviation from the corresponding experimental values are also listed.

Scheelite						HP phase		
ω_{exp} (cm^{-1})	ω_{cal} (cm^{-1})	$\Delta\omega/\omega_{exp}$ (%)	$d\omega/dP$ (cm^{-1} GPa^{-1})	γ_i [a]	Assignment[b]	Notation	ω_c [c] (cm^{-1})	$d\omega_c/dP$ [d] (cm^{-1} GPa^{-1})
75	49	−35	−0.4	−0.66	B_g(T)	ω_1	77	—
102	80	−22	1.3	0.78	E_g(T)			
135	170	26	2.9	1.32	E_g(T)	ω_2	167	—
171	171	0	3.4	1.23	B_g(T)	ω_3	208	2.0
190	183	−4	4.4	1.42	A_g(R)	ω_4	243	2.7
238	222	−7	6.8	1.76	E_g(R)			
337	280	−17	3.3	0.60	$B_g(\nu 2)$	ω_5	361	—
337	360	7	3.3	0.60	$A_g(\nu 2)$	ω_6	383	—
371	371	0	4.1	0.68	$B_g(\nu 4)$	ω_9	444	—
380	389	2	4.6	0.74	$E_g(\nu 4)$	ω_7	446	—
						ω_8	441	6.5
799	799	0	3.0	0.23	$E_g(\nu 3)$	ω_{11}	854	3.9
837	802	−4	2.1	0.15	$B_g(\nu 3)$	ω_{10}	824	—
921	800	−13	2.2	0.15	$A_g(\nu 1)$	ω_{12}	943	2.9

[a] For the determination of γ_i, the value of 61.5 GPa was used for the bulk modulus [4].
[b] From [18].
[c] The ω_c values are determined at 12 GPa.
[d] Missing values indicate strong nonlinear pressure response of the corresponding mode.

coupled via the short-range Lennard-Jones potential,

$$V_{\kappa\kappa'}(r) = V_0\left[\left(\frac{\sigma_\kappa + \sigma_{\kappa'}}{r}\right)^{12} - \left(\frac{\sigma_\kappa + \sigma_{\kappa'}}{r}\right)^{6}\right] \tag{1}$$

where σ_κ, $\sigma_{\kappa'}$ and V_0 are the Lennard-Jones parameters describing the equilibrium position and the strength of the interaction between the κ and κ' atoms in the crystal. Using this potential we have calculated the dynamical matrix and then block-diagonalized it by a similarity transformation using a suitable set of symmetry coordinates.

These short-range interactions are described by a set of five parameters: σ_κ parameters corresponding to Sr, W and O atoms and V_0 parameters corresponding to the strength of the W–O and Sr–O bonds. Their values are determined by least-squares fitting to all measured Raman frequencies in our experiment. The calculated parameters are $\sigma_{Sr} = 1.337$ Å, $\sigma_W = 0.857$ Å, $\sigma_O = 0.797$ Å, $V_{W-O} = 11.521$ eV and $V_{Sr-O} = 4.472$ eV. In table 1 the calculated frequencies are summarized along with the experimental values and their relative deviations. The calculated frequencies exhibit discrepancies ranging from 0 to 35%. It is significant that the large deviations are found in the low-frequency B_g(T), E_g(T) and E_g(T) external modes at 75, 102 and 135 cm^{-1}. This is anticipated since these modes correspond to translational (lattice) motions involving atoms beyond second neighbours, such as the displacements of whole WO_4^{2-} units against each other. These modes have also contributions from long-range (Coulomb) interactions and angular forces and cannot be approximated by the simplified Lennard-Jones potential of equation (1). In contrast, the deviations are smaller in the case of the internal modes $B_g(\nu_2)$ mode at 337 cm^{-1} and the high-frequency $A_g(\nu_1)$ mode at 921 cm^{-1} since these involve mainly short-range interactions within the WO_4^{2-} unit. Therefore, the discrepancies between experimental and calculated frequencies are not surprising, as we have used an empirical model with a minimum number of parameters, which underestimates significantly the Coulomb

interactions. Indeed, in the RIM calculation for $CaWO_4$ [14], where the long-range Coulomb interactions are included, these discrepancies are significantly reduced. At this point, we should point out that our model merely fits the parameters of the imposed potential to the experimentally observed Raman frequencies. Obviously, this approach does not insure the stability of the structure for the resulting parameter values via an energy minimization route. Of course, the use of a more elaborate model is expected to improve the accuracy of the calculated eigenfrequencies as well as that of the eigenvectors, which, as it is known, depend on the applied model. However, we do not expect such changes to result in cancelling of the qualitative characteristics necessary for the discussion concerning the proposed phase transition mechanism. A complete calculation of structural stability and other material properties would be highly favoured, but it is beyond the scope of this study. Our primary aim is to use a simple model, which on one hand reproduces the tendency in the observed Raman frequencies, and on the other hand allows us to determine the mode eigenvectors. Although the frequency distribution of the Grüneisen parameters in table 1 indicates a hierarchy in the strength of the interactions, the fact that they span only one order of magnitude suggests that this hierarchy is not so pronounced. This further implies that our simple model, with only five parameters, can account for a reasonable description of our system.

The calculated bond stretching (L) and bond bending (T) force constants are 453 N m^{-1} (L) and 19 N m^{-1} (T) for W–O bonds and 92 N m^{-1} (L) and 4 N m^{-1} (T) for Sr–O bonds. These values are consistent with our expectation, namely that the W–O bond is stronger than the Sr–O one and the bending force constants are significantly smaller than the stretching ones. The calculated tendency is in accordance with XRD high-pressure measurements [10], which revealed that the compressibility of these materials is mainly due to the compressibility of the longer and softer cation–oxygen bonds ($\sim$2.55 Å) rather than to the shorter and stronger WO_4 tetrahedral bonds ($\sim$1.85 Å).

The calculated eigenvectors for the Raman active modes in the primitive cell of $SrWO_4$ viewed along the a-axis of the crystallographic system are illustrated in figure 3. They are grouped according to their symmetry and in increasing frequency. Note that for the E_g modes, only the one transforming according to the first line of the doubly degenerate irreducible representation is presented. The O atoms, which are not linked with a bond to the nearest W atom, belong to the tetrahedra of neighbouring primitive cells and are equivalent to the bonded atom that does not appear due to the selection of the primitive cell.

The most easily distinguishable modes in figure 3 are those of A_g symmetry, which involve only movement of the oxygen atoms. They originate from the ν_1 (stretching) and ν_2 (quadrupolar) as well as from the rotational (R) tetrahedral modes [19]. Especially for the totally symmetric radial ν_1 mode of WO_4, it can be seen that the presence of the lattice leaves it almost undistorted. For all modes with B_g symmetry, the Sr and W cations move in phase or anti-phase along the c-axis whereas the oxygen atoms have, in general, components along all three axes. In the case of $B_g(\nu_2)$ and the low-frequency B_g(T) the oxygen displacement components along the c-axis are large compared to the ones in the (ab) plane. In the $B_g(\nu_3)$ mode, the tetrahedra are deformed, mainly due to the displacement of oxygen atoms along the W–O bonds justifying the high frequency of this mode. This mode should be more sensitive to the environmental alterations of the tetrahedra than the totally symmetric $A_g(\nu_1)$ mode as it involves directional deformations along the c-axis. For the rest of the B_g modes the relative displacements of either the Sr or the W ions are pronounced.

In the light of the above remarks, an assignment can be made for the two lines originating from the initially unresolved $A_g(\nu_2)$ and $B_g(\nu_2)$ modes at 337 cm^{-1}, which are well resolved at $\sim$9.5 GPa and continue in the high-pressure phase marked as ω_5 and ω_6. The A_g modes, involving only oxygen atom displacements, exhibit a smooth behaviour through the phase

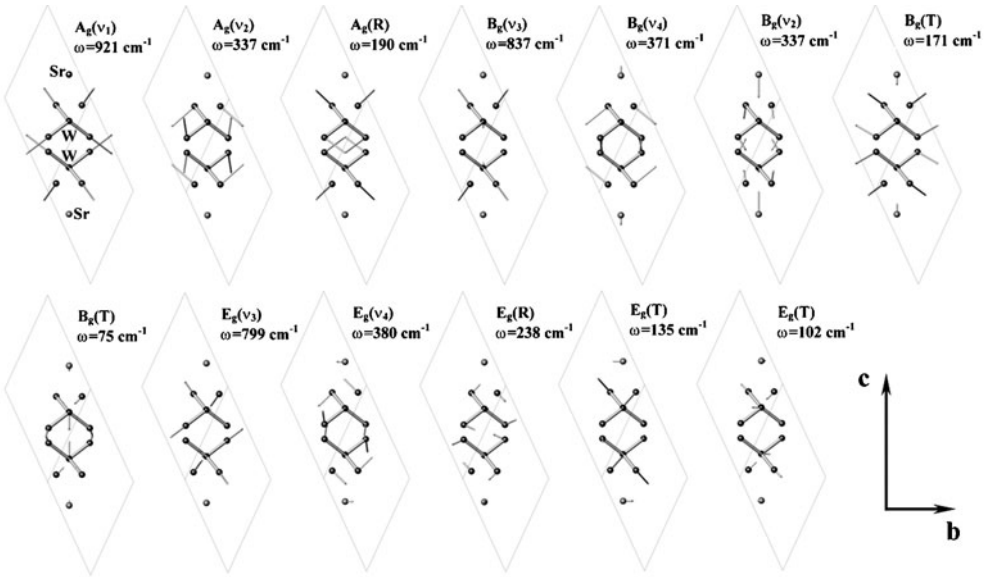

Figure 3. Calculated Raman mode eigenvectors in the primitive cell of $SrWO_4$ viewed along the *a* axis of the crystallographic system. Note that only one of the two degenerate E_g symmetry modes is displayed. Each mode is labelled according to its symmetry and its experimental frequency.

transition. On the other hand the $B_g(\nu_2)$ mode involving large displacement of the Sr atom is more 'anisotropic' and therefore more sensitive to the structural deformations. These considerations lead us to assign tentatively the B_g symmetry to the mode that exhibits a small softening just before the phase transition, marked as ω_5 in the new phase.

The E_g modes are more complicated as they involve movements in planes rather than in specific directions. Nevertheless, the $E_g(\nu_3)$ mode can be clearly seen to involve large displacements in a plane that includes W–O bonds thus justifying its high frequency. In fact the illustrated eigenvectors appear very much as in the case of the $B_g(\nu_3)$ mode but on the (ab) plane. Both Sr and W ions participate in all of these modes and their displacement is restricted on the (ab) plane as dictated by the symmetry. Similarly to the B_g translational modes, the E_g translational modes exhibit relatively large displacements of either the Sr or the W atoms. For example, in the low-frequency B_g(T) mode, the Sr atoms have a displacement amplitude around four to five times smaller than that of W atoms and this ratio becomes even larger for the low-frequency E_g mode. For the other translational modes with higher frequencies, the reverse is true. This result is compatible with the Raman findings for this family of materials where the low-frequency translational modes are more sensitive to the isotopic substitution of the W-type atom whereas the higher-frequency translational modes to the isotopic substitution of the Sr-type atom [18]. Consequently, these modes have been attributed to either Sr-type or W-type ion modes. The strength of the W–O bond, as is evident from our calculation, the experimental Grüneisen parameters and the small alteration of the WO_4 units observed in the high-pressure XRD experiments [10] suggest that the WO_4 anion participates as a whole in these vibrations. In particular, for the low-frequency B_g(T) mode, our calculations show that oxygen atoms 'follow' the displacement of the central atom. In contrast, this does not seem to be the case for the high-frequency B_g(T) mode. Both these modes are expected to originate from the combination of 'acoustic' and 'optical' modes of the chemical unit moving along the *c*-axis. In this case it is expected that the low-frequency phonon would be roughly proportional

to $1/\sqrt{M}$ where $M = M_{Sr} + M_{WO_4}$ while the high-frequency one would be proportional to $1/\sqrt{\mu}$ with $\mu^{-1} = M_{Sr}^{-1} + M_{WO_4}^{-1}$. Then the ratio of the frequencies of the two B_g(T) modes ($171/75 = 2.28$) should be equal to $\sqrt{M/\mu} = 2.276$, which is exactly the case. On the other hand, our calculation indicates that the situation is rather complicated because Sr and W atoms maintain their relative phase, exchanging their amplitudes, while the oxygen atoms in the high-frequency B_g(T) mode have large displacement components in the (ab) plane. In any case, our feeling is that only more elaborate models can tackle such fine and complicated features of some modes.

4. The high-pressure phase

The high-pressure phase and the phase transition mechanism is an important question pertaining to the whole scheelite family which cannot be addressed solely by high-pressure Raman measurements. However, by combining the calculated mode eigenvectors with the pressure behaviour of these modes we can gain valuable information. For example, in the case of $BaWO_4$ [4] (scheelite structure) and $CdWO_4$ [20] (wolframite structure), the ν_1 mode frequency, which represents the totally symmetric W–O stretching vibration, is found to exhibit a large negative jump at the critical pressure. This jump was attributed to a phase transition towards a high-pressure phase in which the central atom has a truly octahedral coordination. This does not appear to be the case for $SrWO_4$ and for other members of the same family [5–8], suggesting that the coordination of W does not change significantly in the new phase.

The slightly higher pressure coefficient of the $E_g(\nu_3)$ mode, compared to that of the $B_g(\nu_3)$ mode in the scheelite phase, can be understood as a pressure induced relative increase of the interaction among the tetrahedra in the (ab) plane with respect to their interaction along the c-axis. The reverse ordering of the frequencies of the $E_g(\nu_3)$ and $B_g(\nu_3)$ modes above 11.5 GPa can be reasonably interpreted, assuming that in the new phase the interaction among tetrahedra in the (ab) plane is stronger than their interaction along the c-axis of the initial structure. However, this picture cannot account for the observed softening in the scheelite phase of the low-frequency B_g(T) mode. The elongation of the c-axis, as a probable cause for this effect, should be ruled out because for other materials of the same family the compressibility along the c-axis is higher than along the a- or the b-axis [10]. Therefore, the cause of this behaviour should be attributed to other effects like deformation and/or tilting of tetrahedra, WO_4 'chain' formation, sliding of layers or the coupling of this mode to an acoustic one.

The wolframite and the monoclinic $BiVO_4$ structures are among the candidates for the high-pressure phase of the scheelite structure found in the literature [4–11, 20–22]. In the wolframite structure, although geometrically described as zig-zag chains of edge-sharing WO_6 octahedra, the WO_4 unit preserves its tetrahedral nature [20, 23] in accordance with our experimental findings for the $A_g(\nu_1)$ mode. The approach of tetrahedra to form these 'chains' and the consequent 'decoupling' of tetrahedra belonging to different chains would be compatible with the aforementioned behaviour of the $B_g(\nu_3)$, $E_g(\nu_3)$ and B_g(T) modes. On the other hand, the monoclinic $BiVO_4$ structure is a deformed scheelite structure where alternating layers along the c-axis of the scheelite structure approach each other forming 'doublets' with a larger spacing between layers belonging to a different doublet [24, 25]. The alternating distance between layers in this structure, in contrast to the initially equidistant layers of the scheelite structure, can also account for the observed behaviour of the internal modes and the low-frequency B_g(T) mode. In fact, the observed softening of the low-frequency B_g mode, in the high-temperature or high-pressure phase transition of the scheelite phase towards the ambient monoclinic structure of this material, has been attributed to its coupling to an acoustic

mode driving the phase transition [26, 27]. The nonlinear behaviour of several Raman modes in the shaded area of figure 2, similar to that observed in $CaWO_4$ [6], could be attributed to the stabilization of the high-pressure phase. On the other hand, the observed instability of the structure might be understood as an intermediate phase, probably involving both the above-mentioned structures or other similar ones. This assumption seems to be the case in $CaMoO_4$, where high-pressure Raman data clearly indicate a sequence of two phase transitions [7]; the only difference in the present case is that the corresponding pressure range between the phase transitions is drastically reduced. Assuming that the high-pressure phase is either that of wolframite or of $BiVO_4$ or even a similar monoclinic structure with C_{2h} point group, the *gerade* modes of the scheelite phase would be transformed in the new phase as follows: $A_g \rightarrow A_g$, $B_g \rightarrow A_g$ and $E_g \rightarrow B_g$. Therefore, the A_g and B_g modes of the scheelite structure, that we were able to follow in our polarized Raman spectra (solid curves in figure 2), should have the A_g symmetry in the high-pressure phase. Indeed, we have resolved eight Raman peaks in the high-pressure phase, exactly as many as expected by group theory. Then, the additional four peaks observed in the unpolarized spectra should have the B_g symmetry. However, their number is less than the ten expected. This could be due to low scattering intensity and/or degeneracies.

5. Conclusion

In conclusion, we report results on the behaviour of Raman modes in $SrWO_4$ single crystals under hydrostatic pressure up to 21 GPa. All modes exhibit changes in their pressure coefficients at the pressure of 11.5 GPa. Above this value and up to 15 GPa the frequencies of several modes exhibit a strong nonlinear behaviour. The theoretical lattice dynamics calculation, although based on a simple empirical potential, reproduces the mode frequencies with reasonable accuracy and permits the illustration of the Raman mode eigenvectors. The calculation justifies the view of a WO_4 unit moving as a 'whole' in the lowest-frequency B_g(T). The pressure behaviour of the internal modes supports the assumption that the tetrahedral nature of the WO_4 unit is preserved through the phase transition until oxygen atoms from the neighbouring units come to a distance such that the central atom senses their presence and is therefore in an effective 'higher' coordination number. A high-pressure phase with deformed WO_4 tetrahedra that preserve their tetrahedral nature is also supported by the reversibility of the high-pressure phase down to ambient pressure. Apart from the wolframite structure where the coordination state of W is compatible with our results, the $BiVO_4$ monoclinic structure should also be considered as a serious candidate for an intermediate or even final high-pressure phase. This could be decided only by x-ray scattering measurements in the high-pressure phase.

References

[1] Voicu G, Bardoux M and Stevensen R 2001 *Ore Geol. Rev.* **18** 211
[2] Faure N, Borel C, Couchaud M, Basset G, Templier R and Wyon C 1996 *Appl. Phys.* B **63** 593
[3] Basiev T T, Sobol A A, Voronko Yu K and Zverev G G 2000 *Opt. Mater.* **15** 205
[4] Jayaraman A, Batlogg B and VanUitert L G 1983 *Phys. Rev.* B **28** 4774
[5] Jayaraman A, Wang S Y and Sharma S K 1995 *Phys. Rev.* B **52** 9886
[6] Christofilos D, Ves S and Kourouklis G A 1996 *Phys. Status Solidi* b **198** 539
[7] Christofilos D, Kourouklis G A and Ves S 1995 *J. Phys. Chem. Solids* **56** 1125
[8] Jayaraman A, Wang S Y, Shieh S R, Sharma S K and Ming L C 1995 *J. Raman Spectrosc.* **26** 451
[9] Shieh S R, Ming L C and Jayaraman A 1996 *J. Phys. Chem. Solids* **57** 205
[10] Hazen R M and Finger L W 1985 *J. Phys. Chem. Solids* **46** 253
[11] Sleight A W 1972 *Acta Crystallogr.* B **28** 2899

[12] Salaun S, Bulou A, Gesland J Y and Simon P 2000 *J. Phys.: Condens. Matter* **12** 7395
[13] Sen S, Chaplot L and Mittal R 2001 *Phys. Rev.* B **64** 024304
[14] Suda J and Sato T 1997 *J. Phys. Soc. Japan* **66** 1707
[15] Sarantopoulou E, Raptis Y S, Zouboulis E and Raptis C 1999 *Phys. Rev.* B **59** 4154
[16] Trotter J, Calvert L D and Gabe E J (ed) 1971 *Structure Reports A* vol 37 (Dordrecht: Reidel) p 252
[17] Hayes W and Loudon R 1978 *Scattering of Light by Crystals* (New York: Wiley) p 103
[18] Liegeois-Duyckaerts M and Tarte P 1972 *Spectrochim. Acta* A **28** 2037
[19] Herzberg G 1945 *Infrared and Raman Spectra of Polyatomic Molecules* (New York: Van Nostrand-Reinhold)
[20] Jayaraman A, Wang S Y and Sharma S K 1995 *Curr. Sci.* **69** 44
[21] Grzechnik A, Syassen K, Loa I, Hanfland M and Gesland J Y 2002 *Phys. Rev.* B **65** 104102
[22] Errandonea D, Somayazulu M and Häusermann D 2002 *Phys. Status Solidi* b **231** R1
[23] Kuzmin A and Purans J 2001 *Radiat. Meas.* **33** 583
[24] David W I F, Glazer A M and Hewat A W 1979 *Phase Transitions* **1** 155
[25] Sleight A W, Chen H-Y, Ferretti A and Cox D E 1979 *Mater. Res. Bull.* **14** 1571
[26] Pinczuk A, Welber B and Dacol F H 1979 *Solid State Commun.* **29** 515
[27] Pinczuk A, Burns G and Dacol F H 1977 *Solid State Commun.* **24** 163